Fuel Optimal Reorientation of Axisymmetric Spacecraft

M. V. DIXON*
The Aerospace Corporation, El Segundo, Calif.
T. N. EDELBAUM†
Charles Stark Draper Laboratory
J. E. POTTER‡ AND W. E. VANDERVELDE§
Massachusetts Institute of Technology, Cambridge, Mass.

The problem of reorienting axisymmetric spacecraft by using reaction control jets and at the same time minimizing fuel expenditure is analyzed. The reorientations considered are not limited to small-angle rotations, and axial cross-coupling is not neglected. However, only rest-to-rest maneuvers are studied and the vehicle is modeled as a rigid body free from disturbance torques. It is assumed that the attitude control thrusters can provide large enough torques for the thrust durations to be negligible compared to the maneuver periods. The Pontryagin Maximum Principle is used to determine the optimality of control profiles involving only two thruster firings—an initial and a terminating thrust. These maneuvers are found to be optimal for a large class of reorientations and this method appears to have great practical potential, typically offering an average spacecraft fuel saving of 10–25% over current techniques.

Nomenclature¶

B = 3×3 matrix of constants, defined by Eq. (46)
b = thruster geometry parameter, defined by Eq. (12)
C = direction cosine matrix
c_x, c_z = thruster exhaust velocities
F = $\partial \mathbf{f}/\partial \boldsymbol{\omega}$
$\mathbf{f}$ = vehicle dynamics
$f_{\xi_f}, f_{\alpha_f}, f_{\beta_f}$ = probability density functions for Euler angles
G = transformation from body to Euler angle rates
$\mathcal{H}$ = Hamiltonian
$\bar{H}$ = angular momentum vector
H = magnitude of angular momentum vector
$\bar{h}$ = unit vector along $\bar{H}$
$(\mathbf{h}x)$ = cross-product matrix, defined as $(\boldsymbol{\omega}x)$ in Eq. (22)
I = 3×3 identity matrix
$\bar{i}_b, \bar{j}_b, \bar{k}_b$ = unit vectors along the vehicle principal axes
$\bar{i}_s, \bar{j}_s, \bar{k}_s$ = unit vectors along the initial vehicle principal axes
J = reorientation cost defined by Eq. (1)
J_x, J_y, J_z = principal-axis vehicle inertias
K = 3×3 matrix defined by Eq. (46)
k = inertia ratio parameter defined by Eq. (7)
P = fuel penalty functions
$R(\phi;\mathbf{h})$ = generalized rotation matrix, performing a rotation of ϕ about unit vector $\mathbf{h}$
r_{ox}, r_{oz} = x and x axis thruster lever arms
t_s, t_f = maneuver start and finish times
t_o = reference time; generally, the midpoint of the maneuver
$\mathbf{u}$ = control accelerations
$\mathbf{u}^*$ = assumed optimal reference trajectory control
Y, Z = 3×3 rotation matrices, performing rotations about the y and z axes, respectively
α, β, ξ = true Euler angles relating the initial and present vehicle orientations
α_f, β_f, ξ_f = the final values of α, β, and ξ
$\delta\boldsymbol{\omega}, \delta\boldsymbol{\xi}$ = transformed state variables, which represent the differences between $\boldsymbol{\omega}$ and $\boldsymbol{\xi}$ on actual and reference trajectories
$\boldsymbol{\theta}$ = small angular differences between actual and reference vehicle orientations measured about the vehicle principal axes
θ = the angle between the vehicle axis of symmetry $\bar{k}_b$ and $\bar{H}$
$\lambda_\omega, \lambda_\xi$ = original costate variables
λ_θ = transformation of λ_ξ
$\lambda_\omega', \lambda_\theta'$ = additional transformations of λ_ω and λ_ξ
$\boldsymbol{\xi} = (\xi, \alpha_f, \beta_f)$ = set of three Euler angles relating the initial and present vehicle orientations
$\boldsymbol{\xi}_f = (\xi_f, \alpha_f, \beta_f)$ = final values of $\boldsymbol{\xi}$
$\boldsymbol{\phi} = (\phi, \theta, \psi)$ = set of rotation angles
ϕ = precessional angle
$\psi, \Delta\psi$ = angular rotations of $\bar{H}$ about $\bar{k}_b$
Ψ_{11}, Ψ_{12} = solutions to costate equations
$\tilde{\omega}$ = vehicle inertial angular velocity in Eq. (2)

Introduction

THE field of spacecraft stabilization in which only vehicle angular velocities are considered is highly developed.[1,2] The more general problem of spacecraft reorientation, where the vehicle orientation is considered as well as its angular velocity, requires three additional state variables such as Euler angles. Most previous investigations[3–7] have been limited to small angular rotations to linearize the Euler angle equations. Numerical optimization techniques can be applied to optimize large-angle reorientations.[8] However, the computation requirements of such procedures are at present prohibitive for onboard calculation. Many current vehicles are reoriented by using a sequence of roll, pitch, and yaw motions. The Apollo Command and Service Module is reoriented with a single rotation about an inertially fixed axis.[9] These techniques will be described in more detail later. They will be compared with the methods proposed here, consisting of initial and final thrust periods separated by a coasting arc.

Received April 4, 1970; revision received July 2, 1970.

* Member of the Technical Staff, Electronics Division, Engineering Science Operations.

† Assistant Director. Associate Fellow AIAA.

‡ Professor, Department of Aeronautics and Astronautics. Member AIAA.

§ Professor, Department of Aeronautics and Astronautics.

¶ Boldface type indicates a 3×1 matrix throughout. Lightface type with overbar indicates a physical 3-dimensional vector throughout.

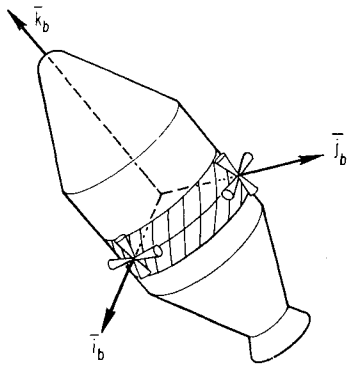

Fig. 1 Typical thruster configuration.

In the present study, the Pontryagin Maximum Principle is used to determine the optimal control logic, which depends on costate variables. The differential equations governing these costate variables are simplified by transformations. When the available control is allowed to become unbounded, the optimal reorientation is shown to consist of a series of coasting periods, separated by impulsive bursts of control. The coasting arc motion of an axisymmetric vehicle is described, and the controls necessary to produce a desired coasting arc are derived. The coasting arc solutions to the costate differential equations can be used to test the (local) optimality of an assumed control impulse sequence. The testing procedure determines when a two-impulse control sequence is (locally) optimal. Finally, a two-impulse method of vehicle reorientation is compared with the current techniques.

Problem Description

Physically, the problem is how to reorient an axisymmetric spacecraft by using reaction control jets and at the same time minimize a maneuver cost. The cost will be considered as proportional to the product of the fuel expenditure and maneuver duration, with the latter assumed to be fixed. However, this time-fuel cost is independent of the maneuver duration. For example, if the maneuver time is doubled, the fuel time is halved, with the basic shape of the trajectory remaining unchanged. The reorientations are not limited to small-angle rotations and axial cross-coupling is not neglected. However, the following assumptions are made. 1) The maneuvers start and terminate with zero angular velocities. 2) For reorientation purposes, the vehicle can be adequately represented as a rigid body, and external disturbance torques may be neglected. 3) The vehicle has two equal principal axis inertias. 4) Vehicle motion during thrusting can be ignored (since the thrusters can provide sufficiently large torques for the thrust durations to be negligible). 5) From any initial vehicle orientation, all final orientations are equally likely.

These assumptions are frequently true in fact. Although the first is not essential to the analysis, spacecraft tasks often require rest-to-rest reorientations. Generally, vehicle bending modes and external disturbance torques do not appreciably affect spacecraft reorientations. In addition, most common spacecraft are approximately axisymmetric. If a vehicle is not perfectly axisymmetric, control torques can be applied to remove the nonaxisymmetric axial cross-coupling effects.

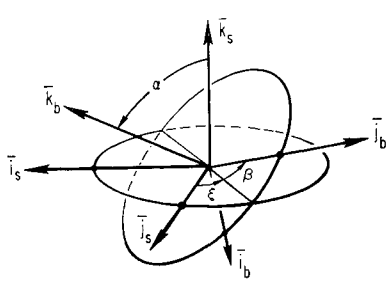

Fig. 2 Euler angle definition.

In general, the fourth assumption is reasonable, because the attitude control thrusters, which must be large to reorient the vehicle rapidly during re-entry and emergencies when fired in short bursts, normally provide adequate torque for reorientations. For example, the thrust periods for the Apollo vehicle are in milli-seconds whereas the reorientations typically take tens of seconds. The final assumption is used to derive an average reorientation cost, which allows a comparison of methods regardless of particular missions.

Two-vehicle thruster configurations are considered. Figure 1 shows a typical fixed-thruster configuration; the thrusters are immobile relative to the vehicle and can provide torques only along the principal axes. Figure 1 becomes a gimballed-thruster configuration if the shaded band on which the thrusters are mounted can rotate about axis $\bar{k}_b$; i.e., the torques may be directed either along the vehicle axis of symmetry, or in any direction perpendicular to this axis. Now if the shaded band could rotate about $\bar{k}_b$ and the jet quads could rotate about axes $\bar{i}_b$ and j_b, a spherical thruster configuration would result, capable of providing torques along an axis in any direction.

Mathematical Formulation

Mathematically, the problem can be expressed in five equations. The nondimensional maneuver cost J,

$$J = (t_f - t_s) \int_{t_s}^{t_f} P(\mathbf{u})dt \tag{1}$$

can be minimized subject to the vehicle motion constraints

$$\dot{\boldsymbol{\omega}} = \mathbf{f}(\boldsymbol{\omega}) + \mathbf{u} \tag{2}$$

and

$$\dot{\boldsymbol{\xi}} = \begin{pmatrix} \dot{\xi} \\ \dot{\alpha} \\ \dot{\beta} \end{pmatrix} = G(\boldsymbol{\xi})\boldsymbol{\omega} \tag{3}$$

and their associated boundary conditions

$$\boldsymbol{\omega}(t_s) = \boldsymbol{\omega}(t_f) = \mathbf{0} \tag{4}$$

and

$$\boldsymbol{\xi}(t_s) = \mathbf{0}; \quad \boldsymbol{\xi}(t_f) = \boldsymbol{\xi}_f \text{ (specified)} \tag{5}$$

where

$$\mathbf{f}(\boldsymbol{\omega}) = k\omega_z \begin{pmatrix} \omega_y \\ -\omega_x \\ 0 \end{pmatrix} \tag{6}$$

$$k \equiv 1 - J_z/J_x; \quad J_x = J_y \tag{7}$$

and

$$G(\boldsymbol{\xi}) = -\frac{1}{\sin\alpha} \begin{bmatrix} \cos\beta & -\sin\beta & 0 \\ -\sin\alpha\sin\beta & -\sin\alpha\cos\beta & 0 \\ -\cos\alpha\cos\beta & \cos\alpha\sin\beta & -\sin\alpha \end{bmatrix} \tag{8}$$

The maneuver starts at time t_s and terminates at t_f. Euler's equations [see Eq. (2)] express $\boldsymbol{\omega}$ the components of the vehicle angular velocity along the vehicle principal axes ($\bar{i}_b$, $\bar{j}_b$, $\bar{k}_b$) as a function of the control accelerations $\mathbf{u}$. Euler $\boldsymbol{\xi}$ angles orient these vehicle axes relative to their initial orientation ($\bar{i}_s$, $\bar{j}_s$, $\bar{k}_s$). These angles are illustrated in Fig. 2.

The penalty function $P(\mathbf{u})$ is chosen to be proportional to the mass flow rate so it depends on the thruster configuration. If equal lever arms and exhaust velocities are assumed for the x- and y-axis thrusters, then

$$P(\mathbf{u}) = P_o(\mathbf{u}) = |u_x| + |u_y| + b|u_z| \tag{9}$$

for the fixed (zero-degree-of-freedom) thruster configuration. Because it has a single degree of freedom, the penalty function for the gimballed configuration is

$$P(\mathbf{u}) = P_1(\mathbf{u}) = (u_x^2 + u_y^2)^{1/2} + b|u_z| \tag{10}$$

The penalty function for a two-degree-of-freedom spherical configuration is

$$P(\mathbf{u}) = P_2(\mathbf{u}) = (u_x^2 + u_y^2 + b^2u_z^2)^{1/2} \tag{11}$$

where the thruster geometry parameter

$$b \equiv J_z r_{ox} c_x / J_x r_{oz} c_z \tag{12}$$

depends on the inertia ratios, the x- and z-axis lever arms (r_{ox}, r_{oz}), and the exhaust velocities (c_x and c_z).

Cost Minimization

The Pontryagin Maximum Principle is used to test for the (local) optimal control program. The Maximum Principle states that the optimal control program minimizes the Hamiltonian $\mathcal{H}$. The Hamiltonian for the problem is

$$\mathcal{H} = P(\mathbf{u}) + \lambda_\omega{}^T[f(\omega) + \mathbf{u}] + \lambda_\xi{}^T G(\xi)\omega \tag{13}$$

where λ_ω and λ_ξ are considered costate variables and satisfy the differential equations

$$\dot{\lambda}_\omega = -(\partial\mathcal{H}/\partial\omega)^T = -F^T\lambda_\omega - G^T(\xi)\lambda_\xi \tag{14}$$

$$\dot{\lambda}_\xi = -(\partial\mathcal{H}/\partial\xi)^T = -\{\partial[G(\xi)\omega]^T/\partial\xi\}\ \lambda_\xi \tag{15}$$

and

$$F \equiv \frac{\partial \mathbf{f}}{\partial \omega} = k\begin{bmatrix} 0 & +\omega_z & +\omega_y \\ -\omega_z & 0 & -\omega_x \\ 0 & 0 & 0 \end{bmatrix} \tag{16}$$

For the fixed thruster configuration where $P(\mathbf{u})$ is given by Eq. (9), the control $\mathbf{u}^*$, which minimizes the Hamiltonian, satisfies

$$u_j{}^* = \begin{cases} 0 & \text{if } |\lambda_{\omega j}| < b_j \\ -\text{SIGN}\,(\lambda_{\omega j})\ \max(u_j) & \text{if } |\lambda_{\omega j}| > b_j \end{cases} \tag{17}$$

where $\max(u_j)$ is the maximum available control and $j = x, y, z$; $b_x = b_y = 1$; $b_z = b$.

The control logic can be implemented by using the concepts of a switching surface and a velocity costate vector $\bar{\lambda}_\omega$. Consider $\bar{\lambda}_\omega$ and $\bar{u}$ (overbars) as physical vectors, and the matrix scalar product $\lambda_\omega{}^T\mathbf{u}$ in the Hamiltonian as a vector dot product $\bar{\lambda}_\omega \cdot \bar{u}$. Since $\mathbf{u}$ represents the components of vector $\bar{u}$ along the vehicle body axes $(\bar{i}_b, \bar{j}_b, \bar{k}_b)$, then λ_ω must represent the components of $\bar{\lambda}_\omega$ in this same frame. When $\bar{\lambda}_\omega$ lies inside the volume enclosed by the switching surface determined by $P(\mathbf{u})$, no control is used. If $\bar{\lambda}_\omega$ exceeds the surface boundaries, full control is applied in an appropriate direction. The switching surface for the fixed thruster configuration is a rectangular prism shown in Fig. 3; the gimballed engine switching surface is a right circular cylinder shown in Fig. 4. The spherical engine switching surface is an ellipsoid.

Full control is applied when $\bar{\lambda}_\omega$ exceeds the switching surface, and no control is used when $\bar{\lambda}_\omega$ lies within its boundaries; thus, excluding singular controls, the optimal control profile consists of alternating maximum and no-control (coasting) periods.

If the available control is allowed to become unbounded, the optimal control profile consists of a series of (finite area) impulses separated by coasting arcs. In this case, $\bar{\lambda}_\omega$ must touch the switching surface for an optimal control policy to be provided. Since the maximum control is applied when $\bar{\lambda}_\omega$ exceeds the switching surface, an infinite quantity of fuel would be used if $\bar{\lambda}_\omega$ extended beyond the surface bounds for a finite duration. This policy would clearly be nonoptimal because the vehicle dynamics are controllable. When $\bar{\lambda}_\omega$ just touches the switching surface, an appropriate control impulse is applied and $\bar{\lambda}_\omega$ moves within the interior of the surface again. The continuity of the Hamiltonian and costates requires $\bar{\lambda}_\omega$ to touch the surface tangentially at the time interior control impulses occur. (Interior controls are those not occurring at the maneuver start of finish.)

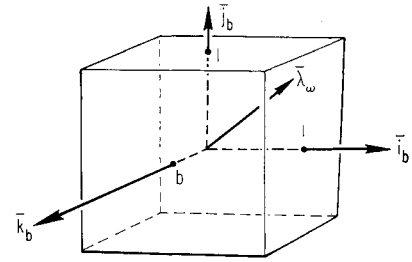

Fig. 3 Fixed engine switching surface.

Costate Transformations

The costate differential Equations (14) and (15) can be simplified by defining new state variables. In the Maximum Principle, only the effect on the cost function J of control variations about the optimal control program is considered. These variations can be large as long as the state variations they produce are of the first order. Therefore, new state variables $\delta\omega$ and $\delta\xi$ are defined as first-order variations about an assumed optimal reference trajectory $\omega(t)$ and $\xi(t)$. From Eqs. (2, 3, and 16), the differential equations governing these new state variables are

$$\delta\dot{\omega} = F(\omega)\delta\omega + (\mathbf{u} - \mathbf{u}^*) \tag{18}$$

and

$$\delta\dot{\xi} = \{\partial[G(\xi)\omega]/\partial\xi\}\delta\xi + G(\xi)\delta\omega \tag{19}$$

where $\mathbf{u}$ is the actual control and $\mathbf{u}^*$ is the assumed optimal reference trajectory control.

From Eq. (3), the differences $\delta\xi$ between the Euler angles on the actual and reference trajectories can be transformed into small angular differences θ about the vehicle principal axes. Thus

$$\theta \equiv G^{-1}(\xi)\delta\xi \tag{20}$$

The differential equation governing θ, which can be obtained from Eqs. (19) and (20), is

$$\dot{\theta} = -(\omega x)\theta + \delta\omega \tag{21}$$

Here, the matrix

$$(\omega x) \equiv \begin{pmatrix} 0 & -\omega_z & \omega_y \\ \omega_z & 0 & -\omega_x \\ -\omega_y & \omega_x & 0 \end{pmatrix} \tag{22}$$

when multiplying a vector $\mathbf{v}$, produces the vector cross-product; that is, $\omega x\mathbf{v} = (\omega x)\mathbf{v}$. Equation (21) implies that (ωx) and G are related by

$$(\omega x) = -(\dot{G}^{-1}G + G^{-1}\{\partial[G(\xi)\omega]/\partial\xi\}G) \tag{23}$$

This relationship can be verified directly, or the differential equation for θ may be derived by using an alternate approach.[10]

Since the new state equations (18) and (21) are linear, the new costates λ_ω and λ_θ are adjoint to them. The new costate

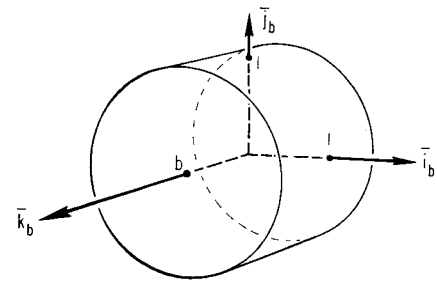

Fig. 4 Gimballed engine switching surface.

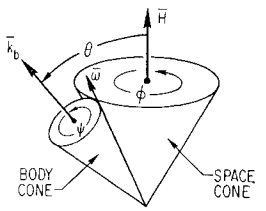

Fig. 5 Coast motion to inertial observer.

differential equations now are

$$\dot{\lambda}_\omega = -F^T\lambda_\omega - \lambda_\theta \qquad \dot{\lambda}_\theta = -(\omega x)\lambda_\theta \tag{24}$$

The velocity costate equations (14) and (24) should be equivalent because the velocity costates λ_ω determine the optimal control program. This equivalence can be proved by using Eqs. (15, 23, and 24) to verify the transformation

$$\lambda_\theta = G^T(\xi)\lambda_\xi \tag{25}$$

Although the costate equations have been simplified, the simultaneous solutions of the coupled state and costate differential equations comprise a formidable problem. It can be solved analytically by allowing the control to become unbounded. From the preceding, the optimal control profile then becomes a sequence of impulses and the reorientation trajectory consists of a series of (patched) coasting arcs.

Coasting Arc Motion

Untorqued rigid-body motion can be described by using the Poinsot construction. For an axisymmetric vehicle with $J_z/J_x < 1$, this consists of two tangent right-circular cones shown in Fig. 5. The vehicle and its axes ($\bar{\imath}_b, \bar{\jmath}_b, \bar{k}_b$) may be considered rigidly attached to the body cone, which rolls without slipping on the space cone, which appears fixed in inertial space.

The axis of the body cone is along the vehicle axis of symmetry $\bar{k}_b$, and the axis of the space cone is along the angular momentum $\bar{H}$. The vehicle angular velocity vector $\bar{\omega}$ is tangent to both cones and lies in the plane determined by $\bar{k}_b$ and $\bar{H}$. The angle ϕ at which $\bar{k}_b$ rotates about $\bar{H}$ is termed the precession angle, and ψ is the angle at which the vehicle axis ($\bar{\imath}_b$ or $\bar{\jmath}_b$) rorates about $\bar{k}_b$. The angles $\boldsymbol{\phi} \equiv (\phi, \theta, \psi)$ satisfy

$$\phi = (H/J_x)(t - t_o) \qquad \theta = \theta(t_o) \tag{26}$$

$$\Delta\psi = \psi - \psi(t_o) = \phi[k/(1-k)]\cos\theta \tag{27}$$

where a reference time t_o is usually set to the starting time t_s and H is the magnitude of the angular momentum.

This dual rotating motion (the vehicle axis of symmetry $\bar{k}_b$ rotating about $\bar{H}$ and the vehicle in turn rotating about $\bar{k}_b$) can be expressed mathematically as

$$C(\phi,\theta,\psi) = Z(\Delta\psi)R(\phi;\mathbf{h}) \tag{28}$$

where C is the direction cosine matrix that relates the vehicle orientations at times t_o and t.

The rotation matrix

$$R(\phi;\mathbf{h}) \equiv \mathbf{h}\mathbf{h}^T + c\phi(I - \mathbf{h}\mathbf{h}^T) - s\phi(\mathbf{h}x) \tag{29}$$

(where c = cosine, s = sine) represents a rotation of angle ϕ about a unit vector in the direction of $\bar{H}$, $\bar{h}$. The (3×1) matrix $\mathbf{h}$ represents the projections of vector $\bar{h}$ (overbar) onto the vehicle axes ($\bar{\imath}_b, \bar{\jmath}_b, \bar{k}_b$) at time t_o; the cross-product matrix

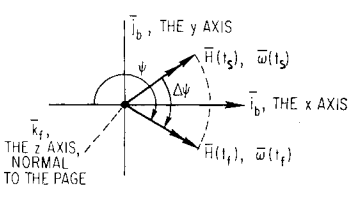

Fig. 6 Coast motion to body observer.

($\mathbf{h}x$) is defined in Eq. (22); and the matrix $Z(\Delta\psi)$ represents the second rotation about the z vehicle axis $\bar{k}_b$. Thus

$$Z(\Delta\psi) \equiv R\left[\Delta\psi;\ \begin{pmatrix}0\\0\\1\end{pmatrix}\right] = \begin{bmatrix} c\Delta\psi & s\Delta\psi & 0 \\ -s\Delta\psi & c\Delta\psi & 0 \\ 0 & 0 & 1 \end{bmatrix} \tag{30}$$

To an observer moving with the vehicle, the angular momentum and angular velocity vectors $\bar{H}$ and $\bar{\omega}$ both appear to rotate about the z vehicle axis, as in Fig. 6. The z-axis components ω_z and H_z are constant. The motion can be described mathematically as

$$\boldsymbol{\omega}(t) = Z(\Delta\psi)\boldsymbol{\omega}(t_o) \tag{31}$$

which is the solution to differential equation (2) for $\boldsymbol{\omega}$. The value of $\boldsymbol{\omega}(t_o)$ is specified by the previous controls, which may be determined from the reorientation geometry ξ_f and the maneuver duration.

Control Calculation

From the laws of dynamics, the change in the angular momentum across a thrust impulse is equal to the integral of the applied torque. These control torques, or equivalently $\bar{H}$, must be calculated from known quantities, such as the Euler angles ξ_f in Eq. (5). These angles specify the direction cosine $C(\xi_f)$, relating the initial and final vehicle orientations, which is

$$C(\xi_f) = Z(\beta_f)Y(\alpha_f)Z(\xi_f) \tag{32}$$

where

$$Y(\alpha_f) \equiv R\left[\alpha_f;\ \begin{pmatrix}0\\1\\0\end{pmatrix}\right] \tag{33}$$

represents a rotation of α_f about the y axis (see Fig. 2). From Eq. (28), this direction cosine matrix can also be expressed in terms of the final values of $\boldsymbol{\phi}$, $\boldsymbol{\phi}_f$ as

$$C(\boldsymbol{\phi}_f) = Z(\Delta\psi_f)R(\boldsymbol{\phi}_f;\mathbf{h}) \tag{34}$$

Here, $\mathbf{h}$, which is the direction of the angular momentum at time t_o, can be expressed in terms of $\boldsymbol{\phi}_f$ (see Figs. 5 and 6) as

$$\mathbf{h} = \frac{1}{H}\begin{bmatrix} J_x\omega_x(t_o) \\ J_y\omega_y(t_o) \\ J_z\omega_z(t_o) \end{bmatrix} = \begin{bmatrix} -s\theta_f & c(\psi_f - \Delta\psi_f) \\ s\theta_f & s(\psi_f - \Delta\psi_f) \\ & c\theta_f \end{bmatrix} \tag{35}$$

The direction cosine matrices $C(\xi_f)$ and $C(\boldsymbol{\phi}_f)$ in Eqs. (32) and (34) represent the same quantities, only expressed in terms of different variables. By equating the traces and skew symmetric components of Eqs. (32) and (34), $\boldsymbol{\phi}_f$ and $\mathbf{h}$ can be expressed as follows in terms of the known Euler angles ξ_f;

$$|c(\boldsymbol{\phi}_f/2)| = c(\alpha_f/2)|c\{[\Delta\psi_f - (\xi_f + \beta_f)]/2\}| \tag{36}$$

$$\Delta\psi_f = \boldsymbol{\phi}_f[k/(1-k)]h_z \tag{37}$$

$$h_x = -(s\alpha_f/2s\boldsymbol{\phi}_f)[s(\xi_f) + s(\Delta\psi_f - \beta_f)] \tag{38}$$

$$h_y = (s\alpha_f/2s\boldsymbol{\phi}_f)[c(\xi_f) + c(\Delta\psi_f - \beta_f)] \tag{39}$$

$$h_z = -[(1 + c\alpha_f)/2s\boldsymbol{\phi}_f]s[\Delta\psi_f - (\xi_f + \beta_f)] \tag{40}$$

The direction of $\bar{h}$, and hence of the control torque, can be determined by first solving numerically the implicit Eqs. (36, 37, and 40) for $\boldsymbol{\phi}_f$ and h_z. There is always at least one set of values for $\boldsymbol{\phi}_f$ and h_z that satisfies these equations[10] when $J_z/J_x < 1$. The values for h_x and h_y may be then calculated directly from $\boldsymbol{\phi}_f$ and h_z by using Eqs. (38) and (39). The magnitude of the control torque is directly proportional to that of the angular momentum $\bar{H}$, which is calculated from $\boldsymbol{\phi}_f$ and the maneuver duration $(t_f - t_o)$ by using Eq. (26).

The controls that are specified by the reorientation geometry ξ_f and the maneuver duration determine the coasting arc reorientation trajectory $\boldsymbol{\omega}(t)$ and $\xi(t)$. Once $\boldsymbol{\omega}(t)$ has been

calculated, the costate differential equations (24), which are functions of $\boldsymbol{\omega}(t)$, can be solved.

Costate Solutions

When the vehicle is on a coasting arc, the solutions to the costate differential equations (24) are

$$\lambda_\omega(t) = Z(\Delta\psi)\lambda_\omega'(t) \tag{41}$$

$$\lambda_\theta(t) = Z(\Delta\psi)\lambda_\Theta'(t) \tag{42}$$

and

$$\begin{pmatrix}\lambda_\omega'(t)\\ \lambda_\theta'(t)\end{pmatrix} = \begin{pmatrix}\Psi_{11}(t,t_o) & \Psi_{12}(t,t_o)\\ 0 & R(\phi;\mathbf{h})\end{pmatrix}\begin{pmatrix}\lambda_\omega'(t_o)\\ \lambda_\theta'(t_o)\end{pmatrix} \tag{43}$$

where

$$\Psi_{11} = I + \phi K(\mathbf{h}x) \tag{44}$$

$$\Psi_{12} = (J_x/H)B[(1 - \cos\phi)(\mathbf{h}x) + (\phi - \sin\phi)(I - \mathbf{h}\mathbf{h}^T) + \phi B^{-1}] \tag{45}$$

$$B = I - K \qquad K = \begin{bmatrix}0 & 0 & 0\\ 0 & 0 & 0\\ 0 & 0 & k\end{bmatrix} \tag{46}$$

The primed costate variables $\bar\lambda_\omega'$ and $\bar\lambda_\theta'$ in Eqs. (41) and (42) represent rotations of $\bar\lambda_\omega$ and $\bar\lambda_\theta$ through an angle $\Delta\psi$ about $\bar k_b$. The expressions for the precession angle ϕ, angular momentum direction $\mathbf{h}$, and the matrices R and Z are given in Eqs. (26, 35, 29, and 30). The form of these costate solutions, and hence of the optimal control policy, does not depend on the maneuver duration.

Control Optimality Test

To determine the optimality of an arbitrary control profile is a formidable task; it may be simplified, however, by allowing the available control to become unbounded. In this case, the optimal control profile consists of a sequence of impulses $\mathbf{u}(t_j)$. The (local) optimality of such an assumed sequence can be tested by first determining the values of the velocity costate vector $\lambda_\omega(t_j)$, which will produce the assumed controls; λ_ω must touch the switching surface at the control times t_j to produce the control impulses. We can calculate $\lambda_\theta(t)$ and $\lambda_\omega(t)$ from the control sequence $\mathbf{u}(t_j)$ and the boundary conditions on $\lambda_\omega(t_j)$ by using their analytical solutions in Eqs. (41–43).

If $\lambda_\omega(t)$ exceeds the switching surface during the maneuver, the assumed control is nonoptimal. If it lies inside the switching surface, touching it only when the assumed control impulses occur, then the assumed profile is an external control. Thus, from a family of control sequences that give rise to neighboring state trajectories (all of which satisfy the state boundary conditions), the assumed control profile results in a stationary value for the maneuver cost J. This value may occur at either a local minimum or a saddle point of J. Extremal two-impulse controls always (locally) minimize the cost J.[10]

The following analysis is limited to reorientations involving only two impulses: an initial thrust to start the maneuver, and a final thrust to terminate the motion. Reorientations involving more than two control impulses have been investigated[10] but proved to be extremal controls in only a few cases. Since the difficulty in calculating the impulse magnitudes and directions required to achieve a desired reorientation increases rapidly with the number of impulses employed, reorientation methods involving more than two may not be practical.

Gimballed Engine Vehicle Reorientations

The optimality of using only an initial and a final control thrust for rest-to-rest reorientations of a gimballed engine vehicle will now be tested. We have seen that these controls can achieve any desired reorientation of an axisymmetric vehicle ($J_x = J_y$; $J_z/J_x < 1$). Briefly, the optimality test procedure just described consists of determining the boundary conditions of λ_ω, $\lambda_\omega(t_s)$, and $\lambda_\omega(t_f)$, which will produce the desired controls. Then $\lambda_\omega(t)$ is calculated. If the assumed control is optimal, a $\bar\lambda_\omega(t)$ trajectory must exist to produce it. Therefore, the control profile is (locally) optimal if $\bar\lambda_\omega(t)$ remains inside the switching surface during the maneuver, thereby producing only the assumed control; otherwise, the assumed control is nonoptimal.

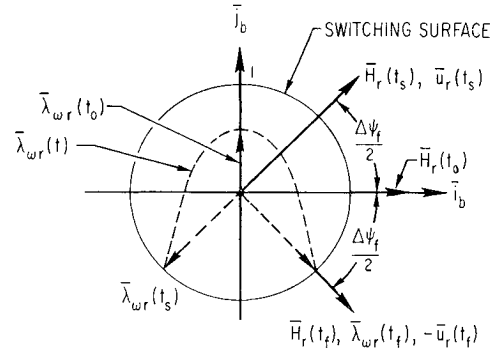

Fig. 7 The $\bar\lambda_{wr}(t)$ trajectory.

The boundary conditions on λ_ω, $\lambda_\omega(t_s)$, and $\lambda_\omega(t_f)$ are chosen to produce the initial and final controls. The final control must null the angular momentum produced by the initial control. It was shown earlier that the angular momentum vector $\bar H$ appears to rotate about the z axis of the vehicle $\bar k_b$, as in Figs. 6 and 7.

In Fig. 7, $\bar H_r$, $\bar\lambda_{\omega r}$, and $\bar u_r$, which are the radial components of $\bar H$, $\bar\lambda_\omega$, and $\bar u$, lie in the plane of $\bar i_b$, $\bar j_b$. For a gimballed thruster configuration $\bar\lambda_{\omega r}$ must be of unit length and along $-\bar u_r$ at the control times t_s and t_f to minimize the Hamiltonian. To take advantage of the gimballed engine configuration symmetry, it will be assumed that the x axis $\bar i_b$ of the vehicle lies along $\bar H_r(t_o)$, where t_o is the midpoint of the maneuver time.

From the geometry in Fig. 7, the boundary conditions on λ_ω are

$$\lambda_\omega(t_s) = \begin{bmatrix}-\cos(\Delta\psi_f/2)\\ -\sin(\Delta\psi_f/2)\\ \mp b\end{bmatrix} = Z^T(\Delta\psi_f/2)\begin{bmatrix}-1\\ 0\\ \mp b\end{bmatrix} \tag{47}$$

and

$$\lambda_\omega(t_f) = \begin{bmatrix}\cos(\Delta\psi_f/2)\\ \sin(\Delta\psi_f/2)\\ \pm b\end{bmatrix} = Z(\Delta\psi_f/2)\begin{bmatrix}+1\\ 0\\ \pm b\end{bmatrix} \tag{48}$$

where $\lambda_{\omega z}(t_s)$ and $\lambda_{\omega z}(t_f)$ must touch the two faces of the switching surface at $+b$ and $-b$ to produce $\omega_z(t_s)$ and null $\omega_z(t_f)$. The sign of ω_z determines the sign associated with b.

For a gimballed vehicle configuration, where the switching surface is symmetrical about $\bar k_b$, $\bar\lambda_\omega'$ can be used to test control

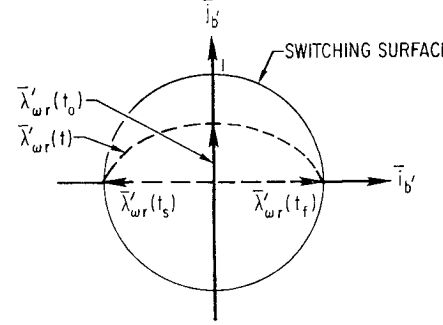

Fig. 8 The $\bar\lambda'_{wr}(t)$ trajectory.

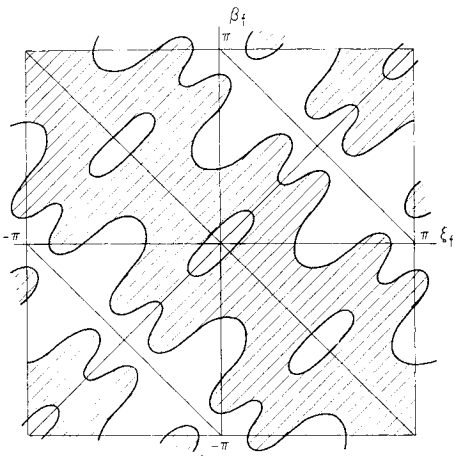

Fig. 9 Two-impulse optimality regions (shaded). (Fixed engine vehicle, $k = 0.7$, $\alpha_f = \pi/2$, $b = J_z/J_x$.)

optimality because $\bar{\lambda}_\omega$ exceeds the switching surface if, and only if, $\bar{\lambda}_\omega'$ exceeds it.

The boundary conditions on λ_ω', $\lambda_\omega'(t_s)$, and $\lambda_\omega'(t_f)$ are obtained immediately from the definition of λ_ω' in Eq. (41) and the boundary conditions on λ_ω in Eqs. (47) and (48). They are

$$\lambda_\omega'(t_s) = \begin{pmatrix} -1 \\ 0 \\ \mp b \end{pmatrix} \qquad \lambda_\omega'(t_f) = \begin{pmatrix} +1 \\ 0 \\ \pm b \end{pmatrix} \tag{49}$$

Here, the midpoint of the maneuver time t_o is set to zero, so that $\phi(t)$ and $\Delta\psi(t)$ in Eqs. (26) and (27) are odd time functions, and angle $\Delta\psi_f/2$ in Eq. (47) is negative. Since $\Delta\psi$ at t_o is zero, $\bar{\lambda}_\omega'(t_o)$ and $\bar{\lambda}_\omega(t_o)$ are equal, as in Fig. 8.

To determine the $\lambda_\omega'(t)$ trajectory, both λ_ω' and λ_θ' must be known at some particular time during the maneuver. Their values at time t_o may be calculated from the expression for $\lambda_\omega'(t)$ in Eq. (43) and the boundary conditions $\lambda_\omega'(t_s)$ and $\lambda_\omega'(t_f)$ in Eqs. (49) as

$$\lambda_\omega'(t_s) = \begin{pmatrix} -1 \\ 0 \\ \mp b \end{pmatrix} = (-\Psi_{11o} + \Psi_{11e})\lambda_\omega'(t_o) + (-\Psi_{12o} + \Psi_{21e})\lambda_\theta'(t_o) \tag{50}$$

and

$$\lambda_\omega'(t_f) = \begin{pmatrix} +1 \\ 0 \\ \pm b \end{pmatrix} = (\Psi_{11o} + \Psi_{11e})\lambda_\omega'(t_o) + (\Psi_{12o} + \Psi_{12e})\lambda_\theta'(t_o) \tag{51}$$

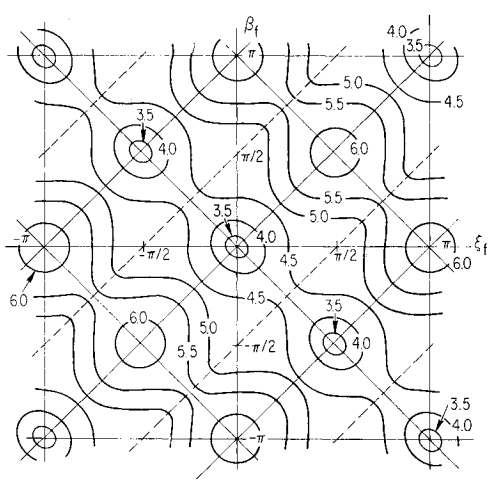

Fig. 10 Two-impulse reorientation cost J. (Fixed engine vehicle, $k = 0.7$, $\alpha_f = \pi/2$, $b = J_z/J_x$.)

where Ψ_{11o}, Ψ_{11e}, Ψ_{12o}, and Ψ_{12e} represent the odd and even times of Ψ_{11} and Ψ_{12} in Eqs. (44) and (45). The angular momentum direction $\mathbf{h}$ in these expressions is evaluated at t_o; thus, h_y equals zero because $\bar{\imath}_b$ was chosen as along $\bar{H}_r(t_o)$.

Since Ψ_{11e} of Eq. (44) is the identity matrix, adding Eqs. (50) and (51) gives

$$\lambda_\omega'(t_o) = -\Psi_{12e}\lambda_\theta'(t_o) \tag{52}$$

Subtracting Eqs. (50) and (51) and substituting Eq. (52) for $\lambda_\omega'(t_o)$ give

$$\lambda_\theta'(t_o) = [-\Psi_{11o}\Psi_{12e} + \Psi_{12o}]^{-1}\begin{pmatrix} 1 \\ 0 \\ \pm b \end{pmatrix} \tag{53}$$

where the determinant

$$\det(\Psi_{11o}\Psi_{12e} + \Psi_{12o}) = -(\phi_f/2)\sin^2(\phi_f/2)\{1 - kh_x^2[1 - (\phi_f/2)/\tan(\phi_f/2)]\} \tag{54}$$

cannot be zero, because the total precession angle ϕ_f always lies between zero and π.[10]

After the values of $\mathbf{h}$ and ϕ_f, which will produce the desired reorientation, are calculated, Eqs. (52) and (53) can be used with Eq. (43) to obtain the unique $\lambda_\omega'(t)$, which will produce the required initial and final controls. The $\lambda_\omega'(t)$ trajectory may be evaluated numerically to determine whether it exceeds the switching surface. In simulations of over 1250 reorientations, every two-impulse reorientation of a gimballed engine vehicle was found to be (locally) optimal. In these simulations, parameter b of Eq. (12) was assumed to be J_z/J_x and the inertia ratio parameter k was varied between zero and unity.

Fixed Engine Vehicle Reorientations

Using the foregoing to ascertain the optimality of two-impulse transfers for a fixed engine vehicle is slightly more difficult. This vehicle has no axis of symmetry, so the true $\lambda_\omega(t)$ must be used in the testing. There is a unique $\lambda_\omega(t)$ that will produce the desired initial and final controls. However, two-impulse fixed engine reorientations are not always (locally) optimal. A map indicating where typically two-impulse reorientations are locally optimal for a fixed engine vehicle ($k = 0.7$; $b = J_z/J_x$; $\alpha_f = \pi/2$) is shown in Fig. 9; Fig. 10 is a reorientation cost J contour map for the same values of k, α_f, and b.

Comparison of Reorientation Methods

Simulation results indicate that for the gimballed thruster configuration, a two-impulse control sequence is locally opti-

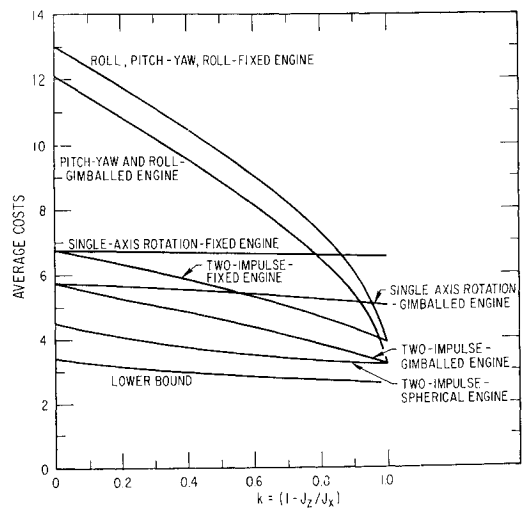

Fig. 11 Average reorientation costs ($b = J_z/J_x$).

mal for a wide class of (if not all) reorientations, as it is also for many fixed engine vehicle reorientations. Unfortunately, this problem is nonlinear, and the Maximum Principle can compare only control sequences that give rise to neighboring trajectories. Two different control sequences, producing different state trajectories that satisfy the same boundary conditions, may both fulfill the local optimality conditions yet have different values of maneuver cost.

Therefore, to determine the practical value of a two-impulse reorientation method, it should be compared with existing techniques. The average costs of the following reorientation methods are compared in Fig. 11. 1) Two-impulse transfers: The control sequence consists of an initial and a final torque impulse. 2) Single-axis rotations: The vehicle is rotated about a single inertially fixed axis to its desired orientation. (This is the method being used for reorienting the Apollo spacecraft.) 3) Roll, pitch-yaw, and roll maneuvers: The general maneuver requires six control impulses: an initial roll and an initial roll terminate; an initial pitch-yaw and a pitch-yaw terminate; a final roll and a final roll terminate. To minimize the maneuver cost, the roll angles and durations are optimized, with the cases of zero initial or final roll being allowed.

The value of the maneuver cost J is a function of four parameters: the three Euler angles ξ_f, α_f, and β_f, and the vehicle inertia k. The (Eq. 12) parameter b was set to J_z/J_x. To present the comparison in the one figure, the maneuver costs were averaged over the Euler angles ξ_f. The Euler angle statistics can be calculated from the assumption that from any initial vehicle orientation, all final orientations are equally likely. These statistics thus become

$$f_{\alpha_f}(x) = sx/2; \quad 0 \leq x \leq \pi \tag{55}$$

$$f_{\xi_f}(y) = f_{\beta_f}(y) = 1/(2\pi); \quad -\pi \leq y \leq +\pi \tag{56}$$

where $f_{\alpha_f}(x)dx$ is the probability that α_f satisfies $x < \alpha_f \leq x + dx$. An average lower bound for the maneuver cost is also plotted in Fig. 11, but cannot be achieved regardless of the reorientation method or thruster configuration. Only the basic vehicle dynamic equations are used in deriving this bound.[10]

Conclusions

The two-impulse method of vehicle reorientation is superior, on the average, to current techniques. In fact, for the gimballed-engine vehicle, individual two-impulse transfers offer a fuel savings in every reorientation over the single-axis rotation and the roll, pitch-yaw, and roll methods, in which only isolated maneuvers were superior for the fixed thruster configuration.

It is not surprising that the two-impulse method offers fuel savings over single-axis rotations or roll, pitch-yaw, and roll maneuvers because such transfers take advantage of the natural vehicle coning motion to complete the reorientation. It is the axial cross-coupling of the vehicle angular velocities in Eq. (2) that causes this coning motion, which single-axis rotations suppress by applying control torques to force the vehicle to rotate about a single axis. Roll, pitch-yaw, and roll maneuvers attempt to avoid axial cross-coupling by performing the rolls and pitch-yaw motions separately; since they are not simultaneous, as in the two-impulse transfer case, they must be faster to complete the reorientation in the prescribed time, and this requires more fuel.

For vehicles with equal inertia ratios (where $J_x = J_y = J_z$; $k = 0$), two-impulse transfers and single-axis rotations are equivalent because there is no axial cross-coupling. Similarly, for rod-shaped vehicles (where $J_z < J_x = J_y$; $k \approx 1$), two-impulse transfers resemble roll, pitch-yaw, and roll maneuvers. However, for a wide range of vehicle inertia ratios, the additional computation required for the two-impulse reorientation method may be more than offset by the considerable average fuel savings.

References

[1] Athans, M. and Falb, P. L., "Time-Optimal Velocity Control of a Spinning Space Body," *IEEE Transactions on Application and Industry*, No. 67, 1963, pp. 206–213.

[2] Ioslovich, I. V., "Optimum Stabilization of a Satellite in an Inertial Coordinate System," *Astronautica Acta*, Vol. 13, No. 11, 1967, pp. 37–47.

[3] Busch, R. E. and Flugge-Lotz, I., "Attitude Control of a Satellite in an Elliptic Orbit," *Journal of Spacecraft and Rockets*, Vol. 4, No. 4, April 1967, pp. 436–442.

[4] Gray, D. L., "Attitude Control of a Satellite in Circular Orbit," *Second IFAC Symposium on Automatic Control in Space*, Instrument Society of America, 1968.

[5] Nishikawa, V., Hayashi, C., and Sannomiya, N., "Fuel and Energy Minimization in Three-Dimensional Attitude Control of an Orbiting Satellite," *Proceedings of the First IFAC Symposium on Automatic Control, in Peaceful Uses of Space*, Plenum Press, New York, 1966, pp. 287–298.

[6] Porcelli, G. and Connolly, A., "Optimal Attitude Control of a Spinning Space Body—a Graphical Approach," *IEEE Transactions on Automatic Control*, Vol. AC-12, June 1967, pp. 241–249.

[7] Studev, R. V., "Some Problems of Optimum Three-Dimensional Attitude Control of Spacecraft," *Proceedings of the First IFAC Symposium on Automatic Control*, Plenum Press, New York, 1966, pp. 268–276.

[8] Hales, K. A. and Flugge-Lotz, I., *Minimum Fuel Attitude Control of a Rigid Body in Orbit by an Extended Method of Steepest Descent*, SUDAR No. 257, Department of Aeronautics and Astronautics, Stanford University, Stanford, Calif., Jan. 1966.

[9] Crisp, R., Keene, D., and Dixon, M., "A Method of Spacecraft Control," *International Astronautical Federation, 17th International Astronautical Congress*, Gordon and Breach, New York, 1967.

[10] Dixon, M. V., "Fuel-Time Optimal Spacecraft Reorientation," T-502, May 1968, Instrumentation Lab., Massachusetts Institute of Technology, Cambridge, Mass.